Science of the Total Environment 737 (2020) 139835

Contents lists available at ScienceDirect

Science of the Total Environment

journal homepage: www.elsevier.com/locate/scitotenv

WRF-Chem simulations of ozone pollution and control strategy in petrochemical industrialized and heavily polluted Lanzhou City, Northwestern China

Jixiang Li [a], Zhanxiang Wang [a], Lulu Chen [a], Lulu Lian [a], Yang Li [a], Liuyuan Zhao [a], Sheng Zhou [a], Xiaoxuan Mao [a], Tao Huang [a], Hong Gao [a], Jianmin Ma [a,b,*]

[a] Key Laboratory for Environmental Pollution Prediction and Control, Gansu Province, College of Earth and Environmental Sciences, Lanzhou University, Lanzhou 730000, PR China
[b] Laboratory for Earth Surface Processes, College of Urban and Environmental Sciences, Peking University, Beijing 100871, PR China

HIGHLIGHTS

- Response of O_3 pollution to precursor chemicals in Lanzhou was simulated.
- Multiple precursor emission control scenarios were implemented in simulations.
- Modeled O_3 formation occurred in VOC and NO_x control regimes in different regions.
- Modeled results provided control strategies for precursor emissions across Lanzhou.

GRAPHICAL ABSTRACT

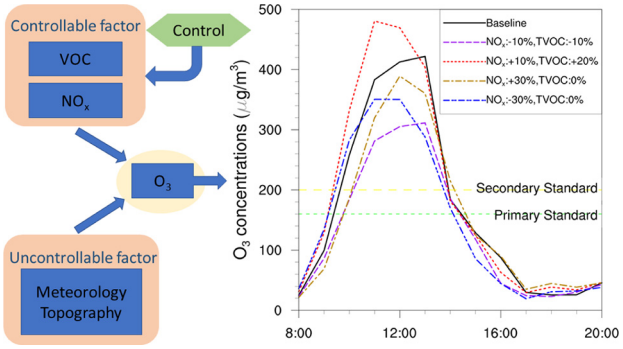

ARTICLE INFO

Article history:
Received 7 February 2020
Received in revised form 20 April 2020
Accepted 28 May 2020
Available online 30 May 2020

Editor: Xinbin Feng

Keywords:
O_3 formation
Precursor chemicals
Emission scenario
Mitigation

ABSTRACT

As the largest petrochemical industrialized city in northwestern China since the 1950s, Lanzhou has been well-known for its heavy surface ozone pollution. Given abundant emission sources of ozone precursors and the favorable environmental conditions for O_3 formation, this study performed extensive atmospheric chemistry modeling investigations subject to 11 emission control scenarios. These scenarios increased and decreased emission levels of total volatile organic compound (TVOC) and nitrogen oxides (NO_x), the two surface ozone (O_3) precursor gases, to examine the relationships between O_3 and NO_x and TVOC. The modeling investigation was carried out for the summer of 2016 in the downtown and petrochemical industrial suburb in the city of Lanzhou. The results revealed that surface O_3 in the downtown area of Lanzhou was controlled by VOCs and in the petrochemical-industrialized western suburb by NO_x. Higher ozone levels were simulated in the west suburb of the city as compared with the downtown area, agreeing with measured data. The relationships between modeled TVOC/NO_x ratios and O_3 reductions, as well as the titration effect, were also discussed. The model results provided useful references for the mitigation strategy of ozone reduction in Lanzhou and other major cities in northwest China with similar climate and topography conditions.

1. Introduction

In recent decades, rapid urbanization and industrialization and the rise in the number of motor vehicles have increased air pollution across

* Corresponding author at: Laboratory for Earth Surface Processes, College of Urban and Environmental Sciences, Peking University, Beijing 100871, PR China.
E-mail address: jmma@pku.edu.cn (J. Ma).

https://doi.org/10.1016/j.scitotenv.2020.139835
0048-9697/

China (Kang et al., 2019; Ning et al., 2018; Sun et al., 2016). Under combined air pollution (Lu et al., 2018), both fine particles and surface O_3 increased and maintained a high level in many areas in China (Duncan et al., 2016; Gao et al., 2017; Ma et al., 2016). Considerable efforts have been made in China to mitigate $PM_{2.5}$ (particulate matter with aerodynamic diameters <2.5 μm) air concentration since 2013 (Wang et al., 2014), which has effectively reduced $PM_{2.5}$ and precursor pollutant (e.g., SO_2 and NO_2) levels across China. In contrast, surface O_3 concentrations have been increasing during the same period, posing a great challenge to the scientific community and local government agents (Lu et al., 2018; Shen et al., 2019). According to the "Annual Environmental Bulletin" issued by the Ministry of Environmental Protection of China (http://www.mee.gov.cn/hjzl/zghjzkgb/lnzghjzkgb/), ozone concentrations exhibited an increasing trend in China from 2013 to 2018. In 2016, the average O_3 concentration reached 138 μg/m^3, and the number of days exceeding the national standard reached 5.2%, increasing by 3% and 0.6%, respectively, from 2015. In summer 2017, the daily maximum 8 h average (MDA8) ozone level exceeding 200 μg/m^3 was measured in 30 major cities across China (CNEMC, 2017). Other field observations and satellites retrieved hourly maximum ozone concentrations in China also frequently exceeded 150 ppb (Li et al., 2017a; Wang et al., 2017). It has been widely recognized that surface ozone has an adverse effect on human health. Exposure to inhaled O_3 may cause oxidative damage and respiratory diseases (Jerrett et al., 2009). As one of the most heavily polluted cities by ozone in China, eye irritation, vegetative damage, and poor visibility have been frequently reported since the mid-1970s (Tang et al., 1989).

Featured by petrochemical and heavy industries constructed from the late 1950s, Lanzhou has been the largest industrialized city in northwestern China. Aged and large-scale industrial facilities, typical mountain-valley topography causing frequently occurring clam winds, strong inversion, heavy traffic, semi-arid climate, and strong sunlight due to relatively high altitude (1530 m above the sea level) all provide an intimate environment for air pollution. Lanzhou has been ranked as one of the top polluted cities based on $PM_{2.5}$ and surface O_3 in China since the 1970s (Feng and Wang, 2012). The first photochemical smog reported in China occurring in the mid-1970s in Lanzhou has been widely recognized as a milestone triggering China's air pollution research (Wang et al., 2009). In the past several years, along with declining $PM_{2.5}$ levels in Lanzhou, owing to strict control measures by the local government, measured O_3 concentrations have been increasing like in eastern and southern China (Li et al., 2019; Xue et al., 2014b). Fig. S1 in Supplementary Information (SI) shows that the annually-averaged $PM_{2.5}$ concentration in Lanzhou declined from 67 to 44 μg/m^3 from 2013 to 2018. In contrast, the annual mean surface O_3 concentration (the daily maximum eight-hour mean concentration with 90th percentile) increased markedly from 92 to 166 μg/m^3, manifesting that O_3 has become the primary criteria air pollutant in the city (Jia et al., 2016). In this context, Lanzhou City, with a population of 3.4 million, provides an opportunity to study ozone pollution and the factors influencing spatial-temporal changes in ozone concentration for those cities with abundant emission sources of precursors and the favorable environment for ozone formation (Chen et al., 1986). It has been known that O_3 is subject to long-range atmospheric transport. Northwestern China has been often experiencing pollutions of air particles and sand storms which could be traced back to the Central-Asia (Kang et al., 2019). Encircled by mountains, the lack of external precursor sources, and frequently occurring calm winds throughout the year in Lanzhou, O_3 atmospheric transport and ventilation effects are not significant. In this context, the city offers a typical environment to isolate atmospheric chemistry and quantify ozone pollution in the city.

Extensive investigations have been carried out to elucidate ozone formation and pollution, and explore control strategies across China (Chang et al., 2017; Hidy, 2000; Lin et al., 2017), of which Lanzhou City was paid special attention due to its heavy ozone pollution (Jia et al., 2016, 2018; Xue et al., 2014b). However, previous studies on O_3 pollution and formation in Lanzhou were carried out over five to ten years ago when $PM_{2.5}$ was the primary air pollutant and were based on field observations at a single sampling site. Although these studies identified NO_x and VOC control regimes for O_3 formation in Lanzhou, the lack of VOC measurement data in petrochemical industrial Xigu created large uncertainties in the determination of the contribution of precursors to O_3 formation (Jia et al., 2016). In particular, previous field sampling studies could not quantify the contributions of emission reduction of precursor gases to O_3 formation and reduction. The present modeling study aims (1) to provide a comparative and quantitative evaluation of the causes behind the increasing ozone trend and to fill knowledge gaps in O_3 pollution and its associations with precursor gases, local meteorology, and topography in Lanzhou, and (2) to shed light on ozone pollution mitigation in Lanzhou and provide a reference for ozone pollution control and reduction in other cities of China with large-scale petrochemical industries, heavy precursor gas emissions,

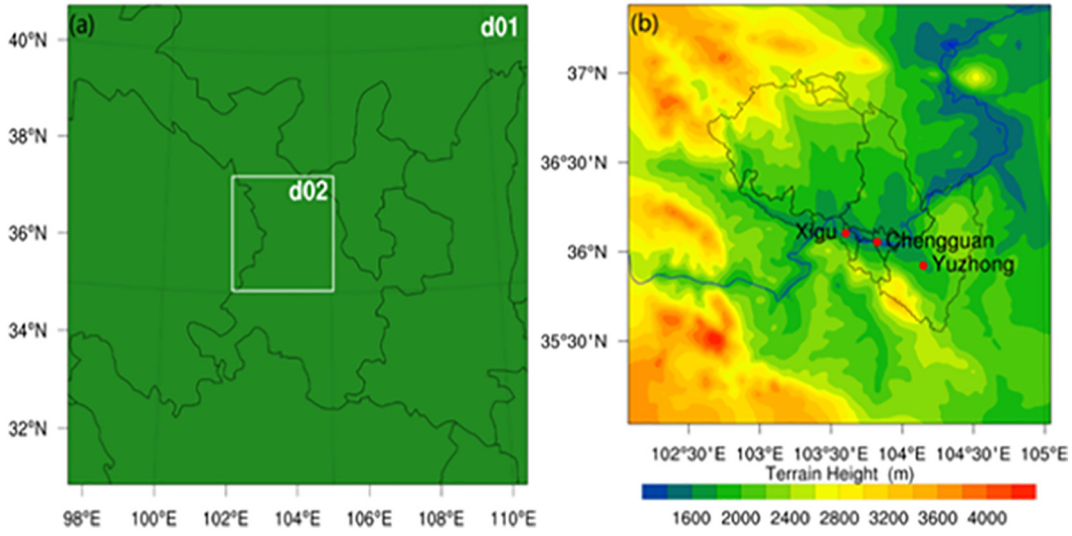

Fig. 1. Model domain (**a**) and terrain height (m) (**b**). The green region in Fig. 1a is the outer domain (d01) that covers most of the Gansu Province and downstream regions, including the Qinghai, Ningxia, Inner Mongolia, Shaanxi, and Sichuan provinces, and d02 is the inner domain covering Lanzhou city and its surroundings. In Fig. 1b, Xingu, Chengguan, and Yuzhong are marked by red dots.

and semi-arid environment, such as the many cities in energy-abundant northwestern China (Ling et al., 2017, 2019; Yang et al., 2018a).

2. Methods and data

2.1. Model setup and configuration

A new generation of the fully coupled regional meteorology-air quality model under an "online" approach WRF-Chem v3.8.1 (Grell et al., 2005) was applied in this model study. The model adopts the Lambert conformal conic projection with two model domains (Fig. 1a and b). Considering complex mountain-valley topography of Lanzhou with the shortest distance in the valley at only about 2 km, to properly predict meteorology and ozone pollution, we selected the spatial resolution of the inner domain as 2 × 2 km. In the WRF-Chem model configuration, the outer domain should not be too small. A grid ratio 5 of the outer domain (10 km) to the inner domain (2 km) spacing was adopted, which took topography, small-scale meteorology and ozone activities, and computational resources into consideration. The outer domain has 124 × 110 model grids, and the inner domain has a 136 × 131 model covering the entire Lanzhou area (Fig. 1). In the vertical, the model atmosphere with the model top at 50 hPa is resolved into 29 layers. The model integration spanned July 1, 2016, to July 14, 2016. The first 40 h of each model scenario simulation was treated as the spin-up time to achieve a quasi-steady state of the meteorological process of the model, such as the cloud process. The model was integrated for 12 days, starting from 1600 GMT on July 2, 2016, to 1500 GMT on July 14, 2016, or 0000 LST (local standard time) on July 3, 2016, to 0000 LST on the 15th, designated for the inner domain only.

The physics parameterization options chosen for this modeling investigation include: (a) a new Rapid Radiative Transfer Model (RRTM) longwave (Mlawer et al., 1997) and a Goddard shortwave (M.-D and Suarez, 1994) radiation scheme; (b) a Morrison double-moment cloud microphysics (Morrison et al., 2009) and an MM5 Monin-Obukhov surface layer scheme (Jiménez et al., 2012); (c) a unified Noah land surface model (Tewari et al., 2004) and MYNN 2.5-level TKE boundary layer physics (Nakanishi and Niino, 2006; Nakanishi and Niino, 2009); and (d) Grell 3D ensemble cumulus parameterization with radiative feedback and shallow convection (Grell and Dévényi, 2002). The Xu-Randall method was used to establish the effect of clouds on the optical thickness. The chemical mechanism uses the MOZART mechanism (Pfister et al., 2011) and has the advantage of simulating the secondary pollution subject to photochemistry. The aerosol chemical process adopts the MOSAIC module, using the KPP library (Zaveri et al., 2008). The Madronich scheme was employed to calculate the TUV photolysis rate (Madronich, 1987), and the dry-wet deposition process used Wesely's scheme (Easter, 2004; Wesely, 1989). WRF-Chem v3.8.1 also provides the option for the two-way feedback mechanism of meteorology and chemicals in the simulation.

2.2. OZIPR simulation

The photochemical model OZIPR (Gery and Crouse, 1991) is a trajectory-based air quality simulation model used in conjunction with the Empirical Kinetics Modeling Approach (EKMA, USEPA) to examine ozone formation subject to VOCs and NO_x emissions. The model has been often used to quantitatively assess the relative importance of non-methane hydrocarbons (NMHCs, or VOCs) and NO_x to the O_3 formation and the sensitivity of O_3 concentration to its precursors, VOCs and NO_x. The inputs of the OZIPR include atmospheric emissions of major ozone precursors VOCs, NO_x, and CO. The OZIPR modeling was performed in the O_3 formation assessment in the Chengguan District due to the availability of sampled VOCs and NO_x data in 2016, but not in Xigu due to the lack of measured VOC data.

2.3. Data

The meteorological data driving WRF-Chem and OZIPR used FNL reanalyzed data with a resolution of 1° × 1° latitude/longitude and a time interval of 6 h. Monthly anthropogenic emissions were obtained from the Multi-resolution Emission Inventory for China (MEIC) (Li et al., 2017b; Zhang et al., 2009) at 0.25° × 0.25° lat/lon resolution in 2016. The allocation of air pollutant emission inventories in space and time is considered. Since the MEIC emission inventory is on a monthly basis, to capture hourly O_3 concentrations subject to hourly changes in precursor chemicals, we assigned 3-hourly emission fractions in the daily emissions of primary gases (SO_2, NO_2, VOCs, CO) based on their respective measured emission and concentration data (Wang et al., 2009). With this practice, we are able to assess the influence of hourly changes in primary emissions, such as the emission in rush hours on ozone pollution. MEGAN biological source data (Guenther et al., 2006) are used. Initial conditions and lateral boundary conditions for each simulated pollutant concentrations were provided by the global atmospheric chemistry model MOZART (Inness et al., 2013).

The measured air concentrations of hourly O_3, NO_x, and CO in the Xigu and Chengguan Districts were collected from official air quality measurement stations in these two districts. More details on the sampling sites and methods are referred to Jia et al. (Jia et al., 2016, 2018). VOCs air concentrations used in OZIPR modeling were measured online using the A52022 series of Gas Chromatography System (C2-C6 A1100 Analyzers, C6-C12 A21022 Analyzers, Chromatotec, France). The instrument is a high-performance gas chromatograph with the FlameIonization Detector (FID) applied in the analysis of VOC compounds (C2-C6 hydrocarbons and BTEX) in gaseous samples (Jia et al., 2016, 2018).

2.4. Model scenarios

It is well-known that ozone concentrations are associated nonlinearly with its precursor gases, typically VOCs and NO_x (Ding et al., 2004). In order to understand the responses of ozone concentrations to altered anthropogenic VOC and NO_x emissions in Lanzhou, the present study simulated the ozone concentrations subject to different VOCs and NO_x emission control scenarios. We set 11 model scenarios, including one baseline scenario (Scenario 0) which used the default total VOC (TVOC) and NO_x emissions collected from the MEIC inventory, and 10 TVOC and NO_x emission control scenarios (Scenarios 1–10) by enhancing and reducing the TVOC and NO_x emission levels by 0–30%, respectively. These scenarios reflect the ozone control measures taken in Lanzhou over the past several years and the likelihood of future VOC and NO_x emission reduction strategies adopted in the next several years. A detailed description of these 11 emission scenarios is presented in Table 1. Considering the sparse vegetation coverage in the semi-arid environment of Lanzhou, and highlighting only the anthropogenic emissions, we incorporated the same BVOC emissions and meteorology in all model scenario runs as we did in the baseline model scenario simulations.

The spatial and temporal changes in the modeled O_3 concentrations from different emission scenarios were statistically assessed and compared, using the temporal and spatial analysis method. The statistical parameters are presented in Table S1 of Supplementary Information (SI). Here, the temporal analysis refers to the Euler method, which picks up the values of interest at a fixed grid cell in chronological order. This method was used to identify potential relationships between ozone and its precursors at a fixed grid cell, aiming to recognize the difference in ozone pollution associated with its precursors in different regions and to assess the influence of the critical areas on O_3 pollution control. Located in the narrow and long Lanzhou Valley with a west-east orientation, two districts of the city were selected to compare the temporal-spatial distribution of ozone concentration. These are the Chengguan District, which features downtown commercial and political

centers in the east of the city, with high population and vehicle densities, and the Xigu District, which features petrochemical and other heavy industries as well as massive emissions to the west of the city (Fig. S1). The two districts are 30 km away from each other. We also selected modeled O_3 concentrations at a grid point in each district to elucidate the temporal variation of O_3 and to examine the causes of O_3 concentration differences between the two districts (Fig. 1b).

2.5. Model evaluation

To verify modeling results, we collected monitored hourly O_3 concentrations from the National Urban Air Quality Real-time Release Platform (http://106.37.208.233:20035/) provided by the Lanzhou Environmental Protection Agency. There are five monitoring sites across Lanzhou City, including four urban sites and one rural station. Table S2 lists the location of these five monitoring sites. Modeled daytime (0800 – 2000 LST) O_3 concentrations from the baseline emission Scenario 0 were evaluated against measured O_3 concentrations at the five official sampling sites using multiple statistical means as presented in Table S1. Considering that the sampling sites do not match exactly with the inner model grids on 2 km resolution (Yang et al., 2018b), we selected four model grid cells approximated mostly in the sampling locations and interpolated the modeled O_3 concentrations to the sampling site location in terms of the weighted distance of each grid to the sampling site.

The statistics between modeled and measured hourly O_3 concentrations in the daytime are presented in Table S2. Figs. S3 and S4 also show the scatter plots and hourly variations, respectively. The results show that the modeled data agree reasonably well with the measured O_3 concentration at the four urban sites, but not for the rural site in Yuzhong (station code 1477A). At this site, the correlation coefficient is 0.268, markedly lower than the urban sites, with r values ranging from 0.46 to 0.64, and the mean difference is -58.85 μg/m^3, suggesting that the model considerably underestimated O_3 concentration at this site. Moreover, the positive values of bias, fraction, and fractional bias among the five sampling sites are only observed at the Qilihe site. At the rest of the sites, these statistical measures are negative. This suggests that the WRF-Chem model tends to overestimate O_3 concentration at the Qilihe site and underestimated it at the rest sampling sites. FA5 (Table S1) ranges from 78%–84% at the five sampling sites with no significant difference, and FA2 (Table S2) shows a significantly lower percentage for all sites.

3. Results and discussion

3.1. Ozone in Chengguan District

Table 1 presents NO_x and TVOC emission control scenarios taken in this study, the statistics of mean daily O_3 concentrations simulated from each emission scenario. In the table we also show the differences of modeled daily O_3 concentrations (μg/m^3) between the emission Scenario 1–10 and baseline scenario (Scenario 0) in the Chengguan District in eastern Lanzhou, defined as $\Delta C_d = C_i - C_0$, where $i = 1, 2, \ldots, 10$ denoting the emission Scenario 1–10, with C_0 as the modeled mean daily O_3 concentration from the baseline emission Scenario 0. Fig. 2 visualizes the difference in modeled daytime (0800 – 2000 LST) (ΔC_d) and hourly (ΔC_h) O_3 concentrations simulated from the emission Scenario 1–10 against the baseline emission Scenario 0. As shown, the most significant changes occurred in emission Scenarios 7 and 8 (NO_x: ±10% TVOC: ±20%). The differences (ΔC_d) and fraction ($F_{CD} = \Delta C_d / C_0$) of the daytime O_3 concentrations show opposite signs between Scenario 7 and 8, with the maximum ΔC_d (6.7 μg/m^3) and F_C (8.79%) from Scenario 7 and the minimum ΔC_d (-9.9 μg/m^3) and F_C (-13.0%) from Scenario 8 among emission control Scenario 1–10 (Figs. 2a and 3a). The daytime concentrations from both scenarios have small standard deviations, as shown in Fig. 2a. These statistics indicate that Scenario 7 and 8 exert the greatest effect on O_3 levels. Especially, ΔC_d of the daytime O_3 from Scenario 8 suggests that this scenario reduces mostly O_3 concentrations in Chengguan among the 10 emission increase and decrease scenarios. ΔC_d from Scenario 1 and 2 (NO_x: ±10%) are both negative, whereas the ΔC_d from Scenarios 3 and 4 (TVOC: ±10%) have opposite signs (Fig. 2), indicating that the effect of TVOC emission on ozone is greater than the effect from NO_x emission. In general, the difference in hourly O_3 concentrations (ΔC_h) also revealed that the effect of TVOC emission exerted a stronger effect on ozone concentrations than that from NO_x (Fig. 2b).

As also shown in Fig. 2b, at most times during the daytime, the increase of TVOC emission enhances ozone concentration, featured by positive ΔC_d and declining TVOC emission leads to the decrease in ozone levels, shown by negative ΔC_d, suggesting a positive response of O_3 concentration to the TVOC emission reduction in the Chengguan District. On the other hand, O_3 concentrations seemed to respond negatively to NO_x emission in the morning ($\Delta C_d < 0$), likely associated with a "NO_x titrated regime" (Xue et al., 2014a). In the afternoon, however, O_3 concentrations generally respond positively to NO_x emissions ($\Delta C_d > 0$). Namely, increasing NO_x emission could enhance O_3 formation in the presence of VOC. It is worth noting that the influence of TVOC on O_3 formation appears stronger in the morning than that in the afternoon, likely related to the highest concentration of ozone at the noontime. The changes in simulated O_3 concentrations subject to the TVOC and NO_x emission control Scenario 5 and 6 (NO_x: ±10% TVOC: ±10%) are similar to those from Scenario 3 and 4 but with smaller ΔC_d values, indicating that the effect of the NO_x and TVOC emission reduction on O_3 variation is less significant than that from Scenario 3 and 4. This reflects the effects of both VOCs and NO_x control regime on ozone formation. The ΔC_d in the emission Scenarios 9 and 10 (NO_x: ±30%) are both negative, and the ΔC_d from Scenario 10 is similar to that of Scenario 8 (Fig. 2a), which is considerably larger than that from the other emission reduction scenarios. The hourly variation in the O_3 concentration from Scenarios 9 and 10 is more or less identical to that from Scenarios 1 and 2, but it shows a stronger positive effect. This turns out that if the NO_x emission reduction is less significant, the NO_x-titrated effect on ozone formation might be stronger.

The fraction ($F_{CD} = \Delta C_d / C_0$) of modeled daytime O_3 concentrations in Fig. 3a also shows that emission Scenarios 7 and 8 play the most important role in O_3 reduction among the 10 precursor emission control scenarios (1−10). The magnitude of the O_3 changes from Scenario 3 is much larger than that from Scenario 1, which implies that the influence of TVOC on O_3 formation is stronger than that of NO_x. Likewise, F_{CH} ($= \Delta C_{ih} / C_{0h}$, where C_{ih} and C_{0h} are modeled hourly O_3 concentrations subject to emission Scenario 1–10 and baseline Scenario 0, respectively) also suggests that TVOC emissions made a greater contribution to

Table 1
NO_x and TVOC emission control Scenarios 0–10, the daily concentration differences (ΔC_d) between emission control Scenarios 1–10 and Scenario 0, and their respective standard deviation (STD) in Chengguan District.

Case	0	1	2	3	4	5	6	7	8	9	10
Change in NO_x (%)	0	10	−10	0	0	10	−10	10	−10	30	−30
Change in TVOC (%)	0	0	0	10	−10	10	−10	20	−20	0	0
ΔC_d (daily, μg/m^3)	0	−2.25	−2.17	2.68	−3.31	1.48	−3.35	3.00	−5.70	−1.25	−5.44
STD (daily, μg/m^3)	0	20.8	15.9	22.9	23.1	28.1	21.1	17.4	18.9	23.1	23.2

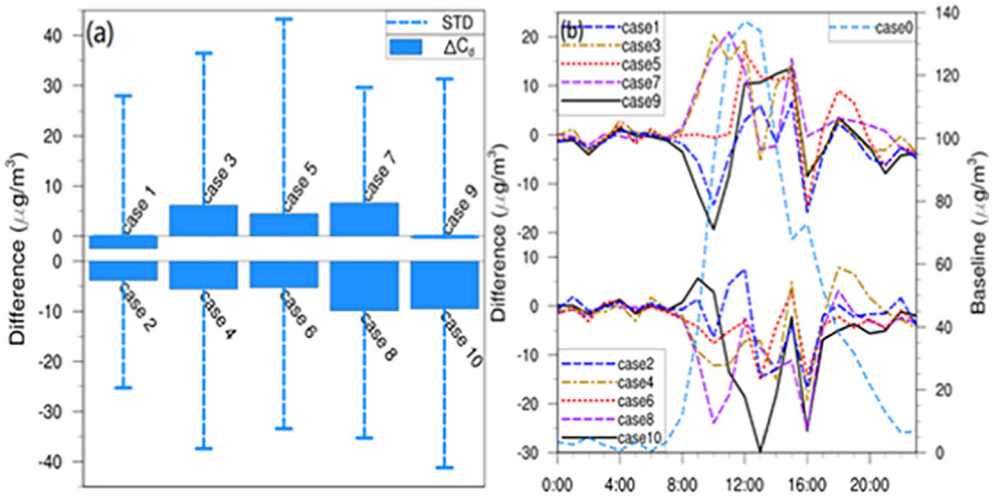

Fig. 2. Daytime ΔC_d (**a**) and ΔC_h (μg/m^3) (b) subject to different precursor emission control scenarios in the Chengguan District.

hourly O_3 fluctuation in Chengguan District than that from NO_x emission.

The hourly changes in F_{CH} were, as expected, consistent with ΔC_{ih} in the afternoon, as shown by increasing ΔC_{ih} and F_{CH} from 1400 to 1500 LST and decreasing ΔC_{ih} and F_{CH} from 1500 to 1600 LST, but didn't match with ΔC_{ih} in the morning time, although F_{CH} is defined by $\Delta C_{ih}/C_{0h}$. For example, no significant decline of F_{CH} from 0800 to 1000 LST is observed, while ΔC_{ih} is decreasing during the same period (Fig. 2b). The most remarkable reduction in hourly F_{CH} occurred at 1600 LST for all emission scenarios (Fig. 3b). As aforementioned, each three-hour fraction of daily primary emissions adopted in our modeling study could identify the "rush hour" effect featured by high NO_x and VOC emission in the morning time (Wang et al., 2009). However, no strong fluctuations or increase of ΔC_{ih} or F_{CH} were identified in the morning rush hours (Fig. 2b, Fig. 3b). As shown in Fig. 3a and b, while we increased both NO_x and TVOC emissions by 10% in model Scenario 5, the estimated ΔC_{ih} and F_{CH} were lower than model Scenario 3, which enhanced 10% TVOC emission only. Similarly, in the emission reduction scenarios, Scenario 4, which reduced 10% TVOC only, accounted for a larger negative fraction than Scenario 6 (Fig. 3b), which reduced 10% emission for both TVOC and NO_x, suggesting that Scenario 4 resulted in more O_3 reduction than Scenario 6 in the morning hours. This anticipates that, although higher level NO was always modeled and observed in the morning rush hours (Fig. S5), the moderately increasing or decreasing NO_x concentrations would not contribute markedly to the O_3 formation in the city's downtown area. This could be attributed to the VOC sensitive regime in Chengguan District and the lower temperature in the morning, partly due to high altitude in Lanzhou (1530 m).

3.2. Peak ozone episode in Chengguan District

We further examined the association between O_3 concentrations and the NO_x and TVOC emissions on July 4, 2016, during which a peak O_3 concentration during the study period (July 3–14, 2016) was simulated. The O_3 concentration reached 422 μg/m^3 at 1300 LST and maintained a high level above 150 μg/m^3 from 1000 to 1400 LST (Fig. 4). Among the 10 precursor emission control scenarios, our modeling result shows that Scenario 6 with a 10% reduction of both TVOC and NO_x emissions performed the best in the decrease in O_3 concentration, particularly in the noontime (1300 LST), as shown by large negative ΔC_h in Fig. 4a. This scenario reduced the maximum O_3 concentration from 422 μg/m^3 to 311 μg/m^3 at 1300 LST, July 4, 2016. Although considered to be the most effective precursor emission control scenario to reduce daily and hourly mean O_3 concentrations in Chengguan District

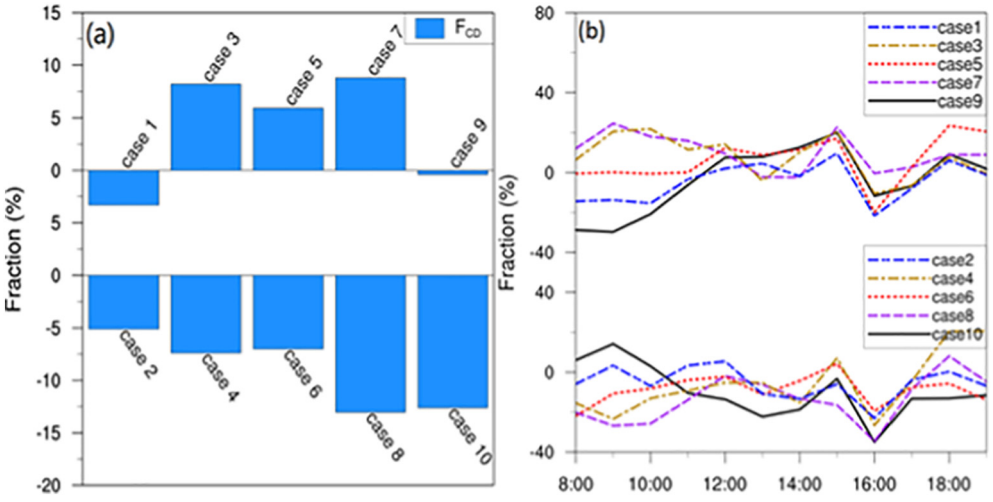

Fig. 3. Daytime fraction (**a**, F_{CD}) and hourly fraction (**b**, F_{CH}) between modeled O_3 concentrations subject to emission control Scenarios 1–10 and baseline Scenario 0 in the Chengguan District.

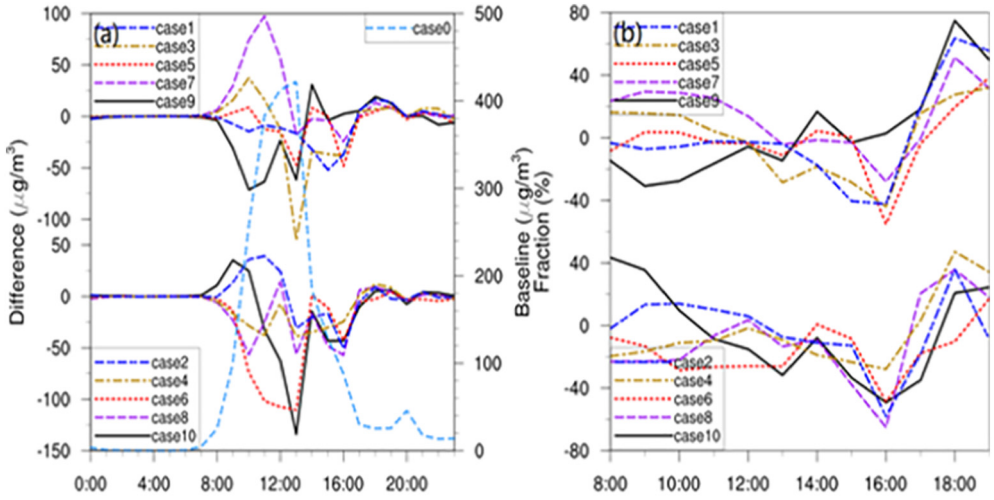

Fig. 4. ΔC_h (**a**) and F_{CH} (**b**) in the Chengguan District on ozone episode day with the maximum concentration of July 3 through 14, 2016.

(Table 1, Figs. 2 and 3), Scenario 8 seemed not to perform equally well as Scenario 6 at the noontime. However, this scenario reduced over 50% O_3 pollution at 1600 LST (Fig. 4b). Surprisingly, emission incline Scenarios 3 and 5 also reduced O_3 levels in the peak O_3 episode day, as shown by ΔC_h at 1300 LST in Fig. 4a and F_{CH} at 1400 LST in Fig. 4b, respectively. As aforementioned, emission control Scenarios 7 and 8 (Figs. 2 and 3) exerted a stronger effect on daytime and hourly O_3 concentrations in Chengguan District than other emission scenarios. In the maximum O_3 level case on July 4, 2016, Scenario 7 yielded the most significant increasing O_3 concentration among the 10 emission control scenarios, enhancing O_3 level by 60–95 μg/m^3 at 1000–1200 LST. Scenarios 7 and 8 showed the greatest effect on the ozone concentration in the morning, followed by Scenarios 3 and 4.

The stronger response of simulated ozone concentrations to TVOC than to NO_x emissions suggests that the Chengguan District could be considered as a NO_x-saturated or VOC-sensitive regime (Lu et al., 2018). Fig. 5 shows the O_3 isopleths averaged from June 30 to July 10, 2016 (Fig. 5a), and on July 3, 2016 with peak O_3 concentration (VOC measurement data was not available after July 10, 2016) in the Chengguan District, simulated by OZIPR model. The straight line in Fig. 5 is referred to as the ridgeline. It denotes the local maxima of the rate of ozone formation. The ridgeline identifies two photochemical regimes. In the NO_x-sensitive regime below the ridgeline, the O_3 increases with the increasing NO_x, and it mirrors relatively little change in the O_3 response to the increasing VOC. In the VOC-sensitive (or NO_x-saturated) regime, the O_3 level rises with the increasing VOC and decreases with the increasing NO_x. Therefore, the O_3 formation tends to be more sensitive to NO_x concentration for a higher VOC/NO_x ratio. In contrast, the O_3 formation is more sensitive to VOC levels when the VOCs/NO_x ratio is relatively lower. As seen in Fig. 5, the slope of the ridgeline is about 23:1, suggesting that ozone is formed in the NO_x control regime for VOCs/NO_x > 23:1 and in the VOC control regime for VOCs/NO_x < 23:1. The sampled mean VOCs/NO_x ratio in Chengguan was 2.36 averaged over the 14-day period (July 1–14, 2016) and 4.11 for the peak O_3 episode day on July 3rd, 2016, respectively, indicating that O_3 was formed in the VOC control regime in the downtown Chengguan District. The result confirms our modeling outcomes that O_3 formation in the Chengguan District tended to be in the VOC-sensitive regime.

3.3. Ozone in Xigu District

Modeled O_3 concentration differences (ΔC_d, μg/m^3) and fractions (F_{CD}, %) between the baseline emission Scenario 0 and Scenarios 1–10 are illustrated in Figs. 6 and **7**, respectively. Similar to the case in the Chengguan District, the precursor emission control Scenario 8 (NO_x: -10%, TVOC: −20%) reduced the most daytime O_3 levels at about −12 μg/m^3, or 16% in Xigu District (Figs. 6a and 7a), followed by Scenario 10 (NO_x: −30%, TVOC: 0%) at about −11 μg/m^3 for ΔC_d and − 15% of F_{CD}. The result seems to suggest that decreasing NO_x emission in the Xigu District might be more effective in the decrease of the O_3 level than reducing the TVOC emission. A comparison of ΔC_d and F_{CD} between Scenario 2 (reducing 10% NO_x only) and Scenario 4 (reducing 10% TVOC only) shows that emission Scenario 2 decreased 8% of O_3 concentration and Scenario 4 decreased 5% of O_3 level in the Xigu District

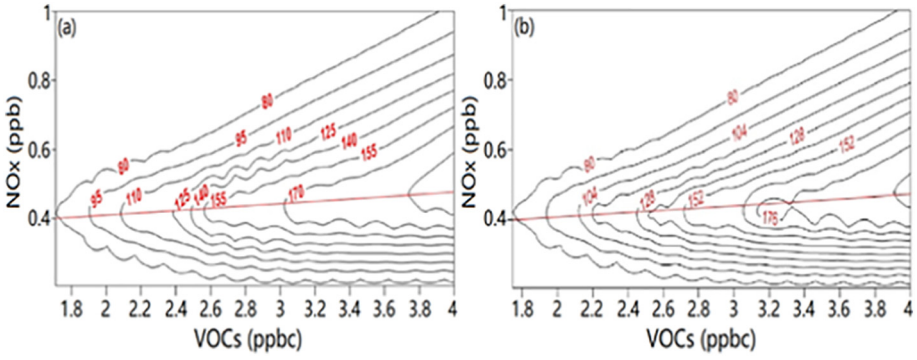

Fig. 5. O_3 isopleths at the official air quality monitoring station in the Chengguan District. (**a**) O_3 isopleths using measured hourly VOCs and NO_x concentrations averaged from May 30 to June 10, 2016; and (**b**) averaged over July 3, 2016.

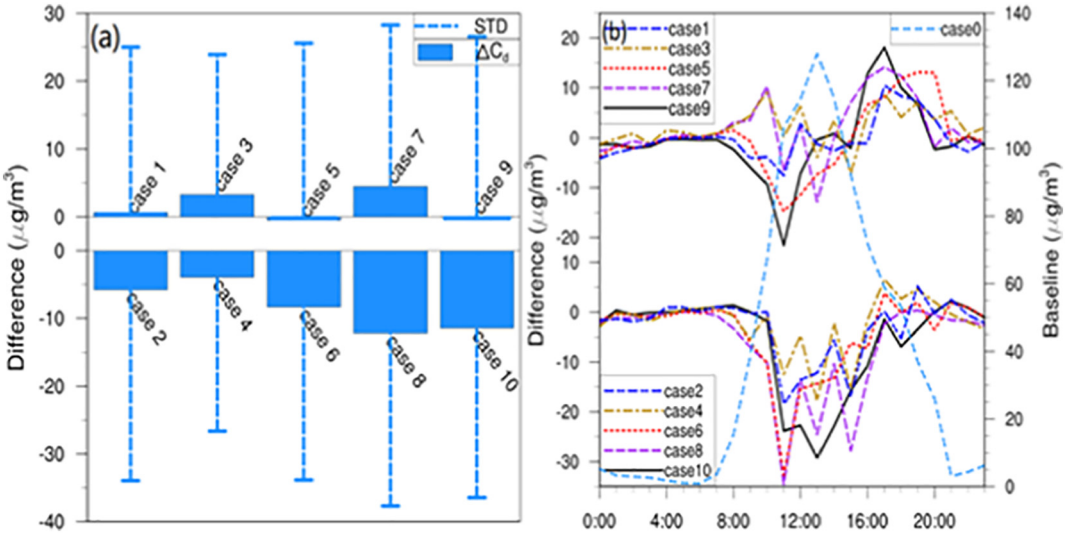

Fig. 6. ΔC_d (daytime O_3 concentration difference μg/m^3), (**a**) and ΔC_h (hourly O_3 concentration difference, μg/m^3) (**b**) subject to different precursor emission control scenarios in the Xigu District.

(Figs. 6a and 7a). The result further demonstrates that the NO_x emission reduction could be a more effective measure to reduce O_3 pollution than TVOC emission reduction.

On the other hand, among those precursor emission enhancement scenarios (Scenario 1, 3, 5, 7, and 9), emission Scenario 7 (NO_x: +10%, VOCs: +20%) and 3 (NO_x: 0%, VOCs: +10%) increased daytime O_3 concentration by about 6% and 4%, respectively, whereas emission Scenario 5 (NO_x: +10%, VOCs: +10%), 1 (NO_x: +10%, TVOC: 0%), and 9 (NO_x: +30%, TVOC: 0%) did not significantly increase daytime O_3 concentrations in the Xigu District (Fig. 6a). Opposite to the precursor emission decreasing scenarios, the emission increasing scenarios suggest that TVOC plays a more important role in the rising daytime ozone than NO_x. For example, the O_3 level increased by 4.4% with increasing TVOC emission by 10% but merely increased 0.8% by increasing 10% NO_x emission (Fig. 7a). Synthesizing the above results, one could conclude that to mitigate O_3 pollution in Xigu District, more effort should be paid to reduce NO_x emission because the increasing O_3 pollution was very likely attributed to the enhancement of NO_x. However, for the cases of increasing precursor chemicals emission, reducing VOC emission is likely a more effective measure to decline O_3 pollution in Xigu.

Like the Chengguan cases (Fig. 3b), the hourly O_3 concentrations in Xigu also show strong fluctuations in the noon and afternoon time, as illustrated in hourly ΔC_h values of the precursor emission control Scenarios 1–10 against the baseline Scenario 0 (Fig. 6b). Differing from the Chengguan cases (Fig. 3b), all ΔC_h values in those emission reduction scenarios decline from the noontime with the largest negative values in Scenarios 8 and 6 at 1100 LST, respectively, followed by Scenario 10 at 1300 LST. In those emission incline cases, we also observed negative ΔC_h values around the noontime, such as Scenario 9, showing that the increasing 30% NO_x emission resulted in a decline in O_3 concentration in the noontime but an increase in O_3 levels in the afternoon, characterized by the largest positive ΔC_h value at 1700 LST (Fig. 6b). Overall, both ΔC_h and F_{CH} in precursor emission incline and decline scenarios exhibited an increasing trend during the daytime, as shown in Figs. 6b and 7b, respectively. This implies that the contribution of the growing precursor emissions to O_3 formation tends to increase in the afternoon. In contrast, the contribution of reducing precursor emissions to O_3 pollution might become weaker towards the afternoon in the petrochemical industrial suburb of Lanzhou, which was likely offset by the stronger photochemical reaction in the afternoon.

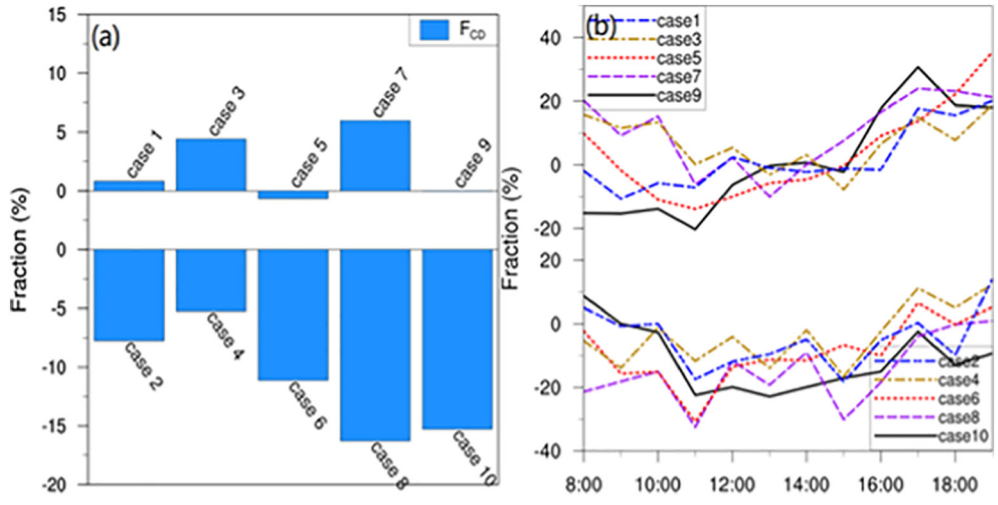

Fig. 7. Daytime F_{CD} (**a**) and hourly F_{CH} (**b**) of O_3 concentrations (μg/m^3) subject to different precursor emission control scenarios of ozone in the Xigu District.

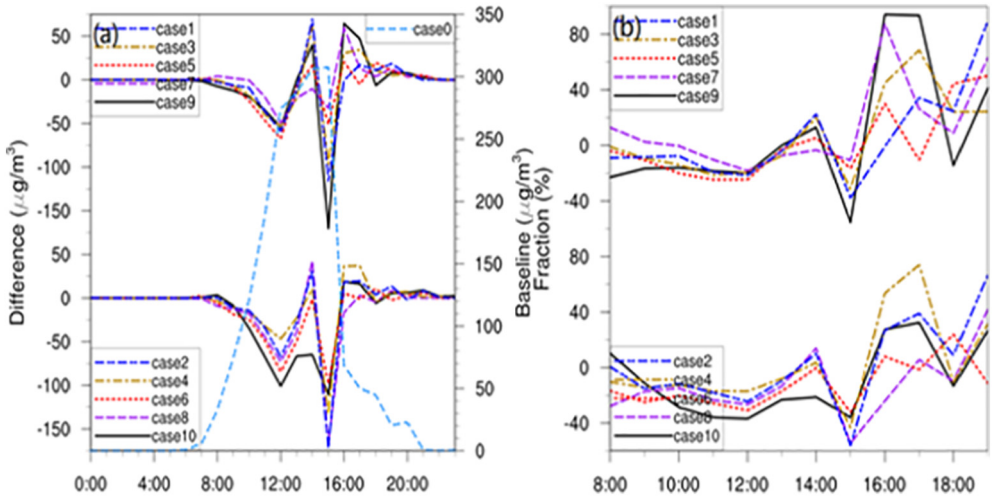

Fig. 8. ΔC_h (μg/m^3) (**a**), and F_{CH} (%) of modeled hourly O_3 concentration between the emission control Scenarios 1–10 and Scenario 0 in Xigu District for the peak ozone day on July 4, 2016.

3.4. Peak ozone episode in Xigu District

The peak ozone episode in Xigu (Fig. S6) during the simulation period also occurred on July 4, 2016, with an hourly maximum of 307 μg/m^3 at 1500 LST and the ozone concentration exceeding 200 μg/m^3 from 1200 to 1600 LST. Fig. 8 shows hourly ΔC_h (Fig. 8a) and F_{CH} (Fig. 8b) values of the modeled O_3 concentrations between emission control Scenarios 1–10 and baseline Scenario 0 (Table 2). The hourly changes in ΔC_h from both emission enhancement scenarios (1, 3, 5, 7, and 9) and reduction scenarios (2, 4, 6, 8, and 10) illustrate a similar pattern, decreasing from 0800 to 1200 LST in the morning, increasing from 1200 to 1400 LST, reducing again and reaching the lowest value at 1500 LST, and little varied (~0) after 1600 LST. Among the five emission reduction scenarios, Scenario 10 reduces mostly the maximum O_3 concentration up to 80 μg/m^3, followed by Scenario 2, which reduces 55 μg/m^3, or 18% of O_3 concentration in the maximum O_3 concentration. While Scenarios 6 and 8 further reduced 10% and 20% TVOC emission (Table 2), these two scenarios yielded a less significant reduction of the peak O_3 concentration than Scenarios 10 and 2. The result confirmed that the ozone formation in Xigu is more sensitive to NO_x emission. This manifests that reducing NO_x emission alone in a heavy O_3 pollution episode might be a cost-effective measure to mitigate O_3 contamination compared to the simultaneous reduction of both NO_x and VOC emission. While marked increasing O_3 concentrations occur in the emission enhancement scenarios at 1400 and 1600 LST (Fig. 8a), significant O_3 reduction can also be observed at 1500 LST, particularly for Scenarios 1 and 9, which increased NO_x emission by 10% and 30% (TVOC: 0%), respectively. These two scenarios reduced O_3 levels up to 30 and 50 μg/m^3.

We found that the emission scenarios 1, 2, 9, and 10 with the fixed TVOC emission all resulted in the decrease of O_3 concentrations, but such decrease responds non-linearly to NO_x emissions. Our results show that the maximum O_3 reduction occurred in Scenario 10 subject to 30% NO_x reduction and the TVOC/NO_x ratio at 1.6, followed by Scenario 1 with 10% increase of NO_x emission and TVOC/NO_x ratio at 0.9, Scenario 2 with 10% NO_x reduction and the TVOC/NO_x ratio of 1.1, and Scenario 9 with 30% increase in NO_x emission and the TVOC/NO_x ratio at 0.8. In general, there is an inverse relationship between the TVOC/NO_x ratios and O_3 concentration reduction. That is, the declining O_3 levels correspond to the increase of TVOC/NO_x ratios and vice versa.

4. Policy implication for O_3 mitigation

Fig. 9 illustrates the spatial distribution of ΔC_d across the Lanzhou Valley between WRF-Chem modeled mean daily O_3 concentration subject to the emission control Scenarios 1–10 and the baseline emission Scenario 0. In general, large ΔC_d values can be found in areas with high O_3 concentrations, and the largest ΔC_d values are identified in Chengguan and Xigu Districts, respectively, the two major source regions of precursor gases due to a large number of vehicles (Chengguan) and large-scale petrochemical and heavy industries (Xigu). Again, Scenarios 7 (NO_x: +10%, TVOC: +20%) and 8 (NO_x: -10%, TVOC: −20%) yielded the largest increasing and decreasing mean O_3 concentration, respectively, occurring mainly in the downtown and western suburb areas. It can also be seen from the figure that in the inner model domain, the influence of VOCs on O_3 pollution was stronger than NO_x.

The responses of O_3 concentrations to the changes in precursor emissions might differ in different places (Xue et al., 2014b). In our case, as can be seen from Fig. 9, the changes in O_3 corresponded better to TVOC reduction in Chengguan District than the other regions across the city. Fig. 9 also shows that in the western suburb (Xigu District), O_3 concentrations respond in a stronger way to NO_x, not to TVOC. For example, the ΔC_{D4} (=C_4 – C_0, where C_4 is the modeled mean O_3 daily concentration from emission Scenario 4, C_0 is the modeled concentration from baseline emission Scenario 0, Fig. 9d) illustrates larger negative values in downtown Chengguan District and smaller negative values in the petrochemical industrialized western suburb (Xigu District). Since this scenario reduced 10% TVOC emission only (Table 2), the different ΔC_{D4} in these two regions suggest that O_3 might respond

Table 2
NO_x and TVOC emission control Scenarios 0–10, the daily concentration differences (ΔC_d) between emission control Scenarios 1–10 and Scenario 0, and their respective standard deviation (STD) in Xigu District.

Case	0	1	2	3	4	5	6	7	8	9	10
Change in NO_x (%)	0	10	−10	0	0	10	−10	10	−10	30	−30
Change in TVOC (%)	0	0	0	10	−10	10	−10	20	−20	0	0
ΔC_d (daily, μg/m^3)	0	−0.17	−3.05	2.24	−2.26	−0.07	−4.40	1.95	−6.63	−0.54	−5.66
STD (daily, μg/m^3)	0	18.3	20.5	15.4	16.7	19.2	18.9	17.6	19.1	19.0	18.9

more strongly to the TVOC emission reduction in the Chengguan District than that in the Xigu District (Fig. 9d). When both NO_x and TVOC emissions were reduced by 10% (Scenario 6, Fig. 9f), we could again obtain greater negative ΔC_D value in the downtown Chengguan District (Fig. 9h). In the case of emission Scenario 10, which reduced 30% NO_x emission, we can observe larger negative ΔC_{D10} in the Xigu District than that in the Chengguan District (Fig. 9j). These results provide evidence and support for the adoption of different O_3 control strategies in different places of the city. Jia et al. (2016) have proposed that to mitigate O_3 pollution in downtown Lanzhou (Chengguan District), the effort should be made to reduce VOC emission, considering that this urban area was in VOC control regime. Our modeling results agree with their conclusions. For Xigu District, however, ΔC_D values seem not to respond strongly to the designated precursor emission reduction scenarios, except for Scenario 10, which reduced 30% NO_x emission. This suggests complex sources of precursor gases in the petrochemical industrialized western suburb. Further studies are needed to investigate the extent of the O_3 response to its precursor gas emissions.

5. Conclusions

Extensive numerical simulations using the WRF-Chem model were conducted to quantify the responses of surface ozone to its primary precursor gases in the downtown and petrochemical industry suburb regions of Lanzhou City in northwestern China. The eleven emission control scenarios, including the baseline emissions collected from the official emission inventory and 10 TVOC and NO_x emission increasing and decreasing scenarios, were implemented into multi-scenario model investigations. Our results showed that ozone level had the largest decline in the downtown (−13%) and the petrochemical industrialized west suburb (−16%) of Lanzhou with 10% and 20% reduction of NO_x and TVOC, respectively. For the peak ozone episode, however, Scenario 6 with a 10% reduction of both TVOC and NO_x emissions reduced 36% O_3 concentration in downtown Lanzhou, whereas Scenario 10 with the reduction of 30% NO_x only performed the best in the decrease in O_3 concentration by 18% in the west suburb of the city. The modeling results identified that O_3 in the downtown Chengguan District was formed in the VOC control regime, agreeing with ozone isopleths obtained using the OZIPR model and measured VOC and NO_x concentrations collected from the official air quality monitoring station in the Chengguan District. In the petrochemical industrial suburb (Xigu), however, our results showed that O_3 model pollution tended to be more sensitive to NO_x in precursor emission reduction scenarios. For increasing TVOC and NO_x emission scenarios, the enhancement of O_3 pollution tended to respond more strongly to the changes in TVOC emission. Overall, our modeling investigation manifested that the ozone was formed very likely in different precursor control regimes in Lanzhou. This could make it difficult to mitigate O_3 pollution in the city. Different emission control strategies are recommended and taken to reduce O_3 pollution in Lanzhou effectively.

It is worth noting that the present study didn't discuss the influences of meteorological and topographic conditions in Lanzhou on O_3 production. As aforementioned in the Introduction, these conditions particularly favor O_3 formation and growth and other air pollutants, which have been extensively investigated (e.g., Wang et al., 2009). Given the lack of measured hourly VOC data in Xigu, the OZIPR simulation was only performed for the downtown Chengguan area to verify the WRF-Chem sensitivity simulations for O_3 to its precursors but not for petrochemical industrial Xigu area. However, the stronger responses of O_3 pollution to NO_x in Xigu obtained from this modeling investigation were consistent with the previous results of Xue et al. (2014a) and Jia et al. (2016). The modeling results revealed that, in the petrochemically industrialized Xigu region, ozone was formed in the NO_x control regime. This NO_x control regime in the suburb of Lanzhou differs from many Chinese cities, where the ozone production was in the VOC regime (Lu et al., 2018; Wang et al., 2017). This outcome, on the one hand, reflects unique characteristics of ozone pollution, and on the other hand, gives rise to challenges in ozone pollution control in Lanzhou city.

CRediT authorship contribution statement

Jixiang Li: Writing - original draft, Methodology, Formal analysis, Visualization.**Zhanxiang Wang:**Formal analysis, Investigation.**Lulu Chen:** Formal analysis.**Lulu Lian:**Formal analysis.**Yang Li:**Formal analysis,

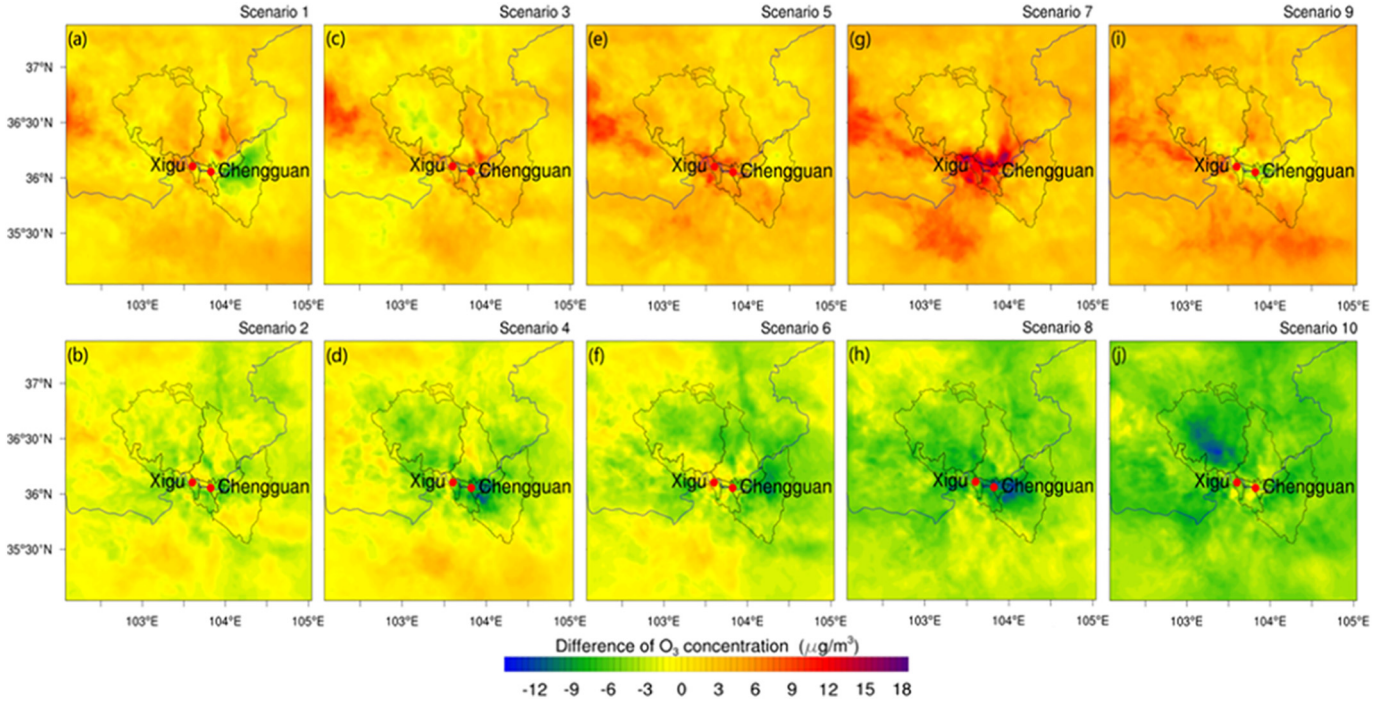

Fig. 9. ΔC_d (μg/m^3) between modeled mean daily O_3 concentrations from the emission control Scenarios 1–10 and the baseline emission Scenario 0.

Investigation.**Liuyuan Zhao:**Formal analysis.**Sheng Zhou:**Formal analysis.**Xiaoxuan Mao:**Formal analysis.**Tao Huang:**Formal analysis.**Hong Gao:**Formal analysis, Investigation, Data curation.**Jianmin Ma:**Conceptualization, Formal analysis, Writing - original draft, Funding acquisition.

Declaration of competing interest

The authors declare that they have no known competing financial interests or personal relationships that could have appeared to influence the work reported in this paper.

Acknowledgment

This work was supported by the National Science Foundation of China (Grants number 41977357 and U1806207) and the Key Project of Gansu Province People's Livelihood Science and Technology (Grant number 1503FCMA003).

Appendix A. Supplementary data

Supplementary data to this article can be found online at https://doi.org/10.1016/j.scitotenv.2020.139835.

References

C, M.-D., Suarez, M.J., 1994. An efficient thermal infrared radiation parameterization for use in general circulation models. NASA Tech. Memo (104606: 85pp).
Chang, K.-L., Petropavlovskikh, I., Cooper, O.R., Schultz, M.G., Wang, T., 2017. Regional trend analysis of surface ozone observations from monitoring networks in eastern North America, Europe and East Asia. Elem. Sci. Anth. 5, 1–22.
Chen, C., Huang, J., Ren, Z., Peng, X., 1986. Meteorological conditions of photochemical smog pollution during sunner in Xigu industrial area, Lanzhou. Acta Sci. Circumst. 6, 334–342.
CNEMC, 2017. Monthly/Quarterly Report of Air Quality of 74 Cities. China National Environmental Monitoring Centre http://www.zhb.gov.cn/hjzl/dqhj/cskqzlzkyb/201711/P020171107495908384256.pdf in Chinese.
Ding, A., Wang, T., Zhao, M., Wang, T., Li, Z., 2004. Simulation of sea-land breezes and a discussion of their implications on the transport of air pollution during a multi-day ozone episode in the Pearl River Delta of China. Atmos. Environ. 38, 6737–6750.
Duncan, B.N., Lamsal, L.N., Thompson, A.M., Yoshida, Y., Lu, Z., Streets, D.G., et al., 2016. A space-based, high-resolution view of notable changes in urban NOx pollution around the world (2005–2014). J. Geophys. Res.-Atmos. 121, 976–996.
Easter, R.C., 2004. MIRAGE: model description and evaluation of aerosols and trace gases. J. Geophys. Res. 109.
Feng, X., Wang, S., 2012. Influence of different weather events on concentrations of particulate matter with different sizes in Lanzhou, China. J. Environ. Sci. 24, 665–674.
Gao, W., Tie, X., Xu, J., Huang, R., Mao, X., Zhou, G., et al., 2017. Long-term trend of O3 in a mega City (Shanghai), China: characteristics, causes, and interactions with precursors. Sci. Total Environ. 603–604, 425–433.
Gery, M., Crouse, R., 1991. User's Guide for Executing OZIPR[M]. US Environmental Protection Agency, Atmospheric Research and Exposure Assessment Laboratory.
Grell, G.A., Dévényi, D., 2002. A generalized approach to parameterizing convection combining ensemble and data assimilation techniques. Geophys. Res. Lett. 29, 38–1–38–4.
Grell, G.A., Peckham, S.E., Schmitz, R., McKeen, S.A., Frost, G., Skamarock, W.C., et al., 2005. Fully coupled "online" chemistry within the WRF model. Atmos. Environ. 39, 6957–6975.
Guenther, A., Karl, T., Harley, P., Wiedinmyer, C., Palmer, P.I., Geron, C., 2006. Estimates of global terrestrial isoprene emissions using MEGAN (Model of Emissions of Gases and Aerosols from Nature). Atmos. Chem. Phys. 6, 3181–3210.
Hidy, G.M., 2000. Ozone process insights from eld experiments part I: overview. Atmos. Environ. 34, 2001–2022.
Inness, A., Baier, F., Benedetti, A., Bouarar, I., Chabrillat, S., Clark, H., et al., 2013. The MACC reanalysis: an 8 yr data set of atmospheric composition. Atmos. Chem. Phys. 13, 4073–4109.
Jerrett, M., Burnett, R.T., Pope, C.A., Ito, K., Thurston, G., Krewski, D., et al., 2009. Long-term ozone exposure and mortality. N. Engl. J. Med. 360, 1085–1095.
Jia, C., Mao, X., Huang, T., Liang, X., Wang, Y., Shen, Y., et al., 2016. Non-methane hydrocarbons (NMHCs) and their contribution to ozone formation potential in a petrochemical industrialized city, Northwest China. Atmos. Res. 169, 225–236.
Jia, C., Wang, Y., Li, Y., Huang, T., Mao, X., Mo, J., et al., 2018. Oxidative capacity and radical chemistry in a semi-arid and petrochemical-industrialized City, Northwest China. Aerosol Air Qual. Res. 18, 1391–1404.
Jiménez, P.A., Dudhia, J., González-Rouco, J.F., Navarro, J., Montávez, J.P., García-Bustamante, E., 2012. A revised scheme for the WRF surface layer formulation. Mon. Weather Rev. 140, 898–918.
Kang, S., Zhang, Q., Qian, Y., Ji, Z., Li, C., Cong, Z., et al., 2019. Linking atmospheric pollution to cryospheric change in the Third Pole region: current progress and future prospects. Natl. Sci. Rev. 6, 796–809.
Li, G., Bei, N., Cao, J., Wu, J., Long, X., Feng, T., et al., 2017a. Widespread and persistent ozone pollution in eastern China during the non-winter season of 2015: observations and source attributions. Atmos. Chem. Phys. 17, 2759–2774.
Li, M., Zhang, Q., Kurokawa, J.-i., Woo, J.-H., He, K., Lu, Z., et al., 2017b. MIX: a mosaic Asian anthropogenic emission inventory under the international collaboration framework of the MICS-Asia and HTAP. Atmos. Chem. Phys. 17, 935–963.
Li, K., Jacob, D.J., Liao, H., Shen, L., Zhang, Q., Bates, K.H., 2019. Anthropogenic drivers of 2013–2017 trends in summer surface ozone in China. Proc. Natl. Acad. Sci. U. S. A. 116, 422–427.
Lin, M., Horowitz, L.W., Payton, R., Fiore, A.M., Tonnesen, G., 2017. US surface ozone trends and extremes from 1980 to 2014: quantifying the roles of rising Asian emissions, domestic controls, wildfires, and climate. Atmos. Chem. Phys. 17, 2943–2970.
Ling, Z., Huang, T., Zhao, Y., Li, J., Zhang, X., Wang, J., et al., 2017. OMI-measured increasing SO2 emissions due to energy industry expansion and relocation in northwestern China. Atmos. Chem. Phys. 17, 9115–9131.
Ling, Z., Huang, T., Li, J., Zhou, S., Lian, L., Wang, J., et al., 2019. Sulfur dioxide pollution and energy justice in Northwestern China embodied in West-East Energy Transmission of China. Appl. Energy 238, 547–560.
Lu, X., Hong, J., Zhang, L., Cooper, O.R., Schultz, M.G., Xu, X., et al., 2018. Severe surface ozone pollution in China: a global perspective. Environ. Sci. Technol. Lett. 5, 487–494.
Ma, Z., Xu, J., Quan, W., Zhang, Z., Lin, W., Xu, X., 2016. Significant increase of surface ozone at a rural site, north of eastern China. Atmos. Chem. Phys. 16, 3969–3977.
Madronich, S., 1987. Photodissociation in the atmosphere, 1, actinic flux and the effects of ground reflections and clouds. J. Geophys. Res. 92, 9740–9752.
Mlawer, E.J., Taubman, S.J., Brown, P.D., Iacono, M.J., Clough, S.A., 1997. Radiative transfer for inhomogeneous atmospheres: RRTM, a validated correlated-k model for the longwave. J. Geophys. Res.-Atmos. 102, 16663–16682.
Morrison, H., Thompson, G., Tatarskii, V., 2009. Impact of cloud microphysics on the development of trailing stratiform precipitation in a simulated squall line: comparison of one- and two-moment schemes. Mon. Weather Rev. 137, 991–1007.
Nakanishi, M., Niino, H., 2006. An improved Mellor–Yamada Level-3 model: its numerical stability and application to a regional prediction of advection fog. Bound.-Layer Meteorol. 119, 397–407.
Nakanishi, M., Niino, H., 2009. Development of an improved turbulence closure model for the atmospheric boundary layer. J. Meteorol. Soc. Jpn. 87, 895–912.
Ning, G., Wang, S., Yim, S.H.L., Li, J., Hu, Y., Shang, Z., et al., 2018. Impact of low-pressure systems on winter heavy air pollution in the northwest Sichuan Basin, China. Atmos. Chem. Phys. 18, 13601–13615.
Pfister, G.G., Avise, J., Wiedinmyer, C., Edwards, D.P., Emmons, L.K., Diskin, G.D., et al., 2011. CO source contribution analysis for California during ARCTAS-CARB. Atmos. Chem. Phys. 11, 7515–7532.
Shen, G., Ru, M., Du, W., Zhu, X., Zhong, Q., Chen, Y., et al., 2019. Impacts of air pollutants from rural Chinese households under the rapid residential energy transition. Nat. Commun. 10.
Sun, L., Xue, L., Wang, T., Gao, J., Ding, A., Cooper, O.R., et al., 2016. Significant increase of summertime ozone at Mount Tai in Central Eastern China. Atmos. Chem. Phys. 16, 10637–10650.
Tang, X.Y., Li, J.L., Dong, Z.X., Wang, Y.Y., Wang, W.X., Qi, L.W., et al., 1989. Photochemical pollution in Lanzhou, China-a case study. J. Environ. Sci. 58, 384–395.
Tewari, M., Chen, F., Wang, W., Dudhia, J., LeMone, M.A., Mitchell, K., et al., 2004. Implementation and verification of the unified NOAH land surface model in the WRF model. 20th Conference on Weather Analysis and Forecasting/16th Conference on Numerical Weather Prediction, pp. 11–15.
Wang, S., Feng, X., Zeng, X., Ma, Y., Shang, K., 2009. A study on variations of concentrations of particulate matter with different sizes in Lanzhou, China. Atmos. Environ. 43, 2823–2828.
Wang, S.X., Zhao, B., Cai, S.Y., Klimont, Z., Nielsen, C.P., Morikawa, T., et al., 2014. Emission trends and mitigation options for air pollutants in East Asia. Atmos. Chem. Phys. 14, 6571–6603.
Wang, T., Xue, L., Brimblecombe, P., Lam, Y.F., Li, L., Zhang, L., 2017. Ozone pollution in China: a review of concentrations, meteorological influences, chemical precursors, and effects. Sci. Total Environ. 575, 1582–1596.
Wesely, M.L., 1989. Parameterization of surface resistances to gaseous dry deposition in regional-scale numerical models. Atmos. Environ. 23, 1293–1304.
Xue, L., Wang, T., Louie, P.K., Luk, C.W., Blake, D.R., Xu, Z., 2014a. Increasing external effects negate local efforts to control ozone air pollution: a case study of Hong Kong and implications for other Chinese cities. Environ. Sci. Technol. 48, 10769–10775.
Xue, L.K., Wang, T., Gao, J., Ding, A.J., Zhou, X.H., Blake, D.R., et al., 2014b. Ground-level ozone in four Chinese cities: precursors, regional transport and heterogeneous processes. Atmos. Chem. Phys. 14, 13175–13188.
Yang, J., Ji, Z., Chen, D., Kang, S., Fu, C., Duan, K., et al., 2018a. Improved land use and leaf area index enhances WRF-3DVAR satellite radiance assimilation: a case study focusing on rainfall simulation in the Shule River Basin during July 2013. Adv. Atmos. Sci. 35, 628–644.
Yang, J., Kang, S., Ji, Z., Chen, D., 2018b. Modeling the origin of anthropogenic black carbon and its climatic effect over the Tibetan plateau and surrounding regions. J. Geophys. Res.-Atmos. 123, 671–692.
Zaveri, R.A., Easter, R.C., Fast, J.D., Peters, L.K., 2008. Model for simulating aerosol interactions and chemistry (MOSAIC). J. Geophys. Res. 113.
Zhang, Q., Streets, D.G., Carmichael, G.R., He, K.B., Huo, H., Kannari, A., et al., 2009. Asian emissions in 2006 for the NASA INTEX-B mission. Atmos. Chem. Phys. 9, 5131–5153.